Raman Line Shapes of Optical Phonons of Different Symmetries in Anatase TiO2 Nanocrystals

ARTICLE *in* THE JOURNAL OF PHYSICAL CHEMISTRY C · SEPTEMBER 2009

Impact Factor: 4.77 · DOI: 10.1021/jp9046193

3 AUTHORS, INCLUDING:

Varadarajan Sridharan
Indira Gandhi Centre for Atomic Research
55 PUBLICATIONS **311** CITATIONS

Raman Line Shapes of Optical Phonons of Different Symmetries in Anatase TiO_2 Nanocrystals

Satyaprakash Sahoo,* A. K. Arora, and V. Sridharan

Material Science Group, Condensed Matter Physics Division, Indira Gandhi Centre for Atomic Research, 603102, India

Received: May 18, 2009; Revised Manuscript Received: August 19, 2009

Raman spectroscopic investigations of phonons of different symmetries in anatase TiO_2 nanocrystals synthesized by the sol−gel method are carried out. Out of six Raman active phonons, the line shapes of two E_g modes and one B_{1g} mode have been analyzed quantitatively to distinguish between the contributions of laser-induced local heating, phonon confinement effects, and defects to the line broadening. The line shape asymmetry arising from confinement of optical phonons in the 397 cm^{-1} B_{1g} mode is found to be of opposite nature than those in the 144 and 639 cm^{-1} E_g modes. This arises due to the negative dispersion of the 397 cm^{-1} B_{1g} phonon dispersion curve. The measured spectra show larger broadening than those predicted by a phonon confinement model. The excess broadening, attributed to intrinsic defects, is found to be least for the 144 cm^{-1} E_g mode and largest for the 397 cm^{-1} B_{1g} mode. In addition, finite laser power of the excitation wavelength is found to raise the temperature of the nanocrystals, with heating being maximum for the smallest size nanocrystals.

Introduction

There is considerable current interest in nanostructured TiO_2 due to numerous applications that include photovoltaic cells, photoactivated catalytic processes, gas sensors, and self-cleaning and biocompatible surfaces.[1,2] Natural TiO_2 exists in three polymorphs: anatase, rutile, and brookite. The tetragonal structure of anatase (space group D_{4h}^{19}) has two formula units per primitive cell, leading to six Raman active phonons: $3E_g$ (144, 196, and 639 cm^{-1}), $2B_{1g}$ (397 and 519 cm^{-1}), and $1A_{1g}$ (513 cm^{-1}). On the other hand, the rutile phase has only four Raman active modes: B_{1g} (143 cm^{-1}), E_g (447 cm^{-1}), A_{1g} (612 cm^{-1}), and B_{2g} (826 cm^{-1}).[3] Nanostructured samples of both anatase and rutile phases and their mixtures have been extensively characterized using Raman spectroscopy.[4−8] Bersani et al. have analyzed the Raman spectra of the 144 cm^{-1} E_g phonon in 10−14 nm anatase nanocrystals using a phonon confinement model.[6] However, the parameters used for calculating the Raman line shapes from the phonon confinement model, in particular the value of the width of the dispersion curve, were completely arbitrary and different from that found from the lattice dynamical calculations. Recently, Bassi et al. have reported the influence of size and stoichiometry on the Raman spectra of titania nanoparticles synthesized by flame pyrolysis[5] and attributed the observed behavior to stoichiometry defects. On the other hand, the line width was less affected by the oxygen content. Furthermore, their samples contained both anatase and rutile phases. It may be pointed out that one of the E_g phonons of anatase and the B_{1g} phonons of the rutile phase appear nearly at 144 cm^{-1}. In view of this, analysis of line width data of a two-phase system based on the phonon dispersion curve of a single phase appears inappropriate. Furthermore, almost all of the investigations carried out so far on phonon confinement in anatase nanoparticles have focused only on the strongest 144 cm^{-1} E_g phonon and no attempt has been made to analyze the phonon of other symmetries. Earlier, it has been shown in the case of ZnO nanoparticles that the consequences of phonon confinement are different for phonons of different symmetries.[9] In view of this, it is worth examining the effect of phonon confinement on the Raman line shapes of the phonons of different symmetries in the anatase TiO_2. It may be pointed out that defects and heating also cause broadening of the Raman spectra. Both of these effects cause symmetric broadening of the line shape. The temperature dependent Raman shift and broadening is usually governed by two mechanisms: thermal expansion and anharmonic coupling of phonons to other phonon branches.[10−12] The anharmonic coupling of phonons can occur in two ways, an optical phonon can symmetrically decay into two acoustic phonons having the same energy but opposite momenta, or it can decay asymmetrically into a transverse optical and a longitudinal acoustic phonon.[13,14] Hence, the consequences of each of these mechanisms on the line shape need to be examined. Here, we report a Raman spectroscopic study of phonons in small-sized anatase nanocrystals. In addition to the 144 cm^{-1} E_g mode, the Raman line shapes of confined optical phonons of other symmetries, such as those of 397 cm^{-1} B_{1g} and the other 639 cm^{-1} E_g mode are analyzed using a Gaussian confinement model. The calculated line shapes are compared with the measured spectra. Apart from phonon confinement, the temperature can also affect the Raman line width and the peak position.[15] The effect of laser-induced local heating on the Raman line shape of nanoparticles is also examined in detail.

Experimental Details and Line Shape Calculation

The synthesis of TiO_2 nanoparticles was carried out using a procedure similar to that reported by Li et al.[16] To 500 mL of ethanol, kept in an ice bath, nearly 50 mL of $TiCl_4$ was poured drop by drop, resulting in a clear solution. The solution was stirred at room temperature for 60 min, and it was then heated at 80 °C for 3 days to yield white powder. The powder was washed several times and again dired at 80 °C for 2 days. The as-synthesized powder was annealed at temperatures between

* Author to whom correspondence should be addressed. E-mail: satyasahoo@igcar.gov.in, satya504@gmail.com. Phone: +91-44-27480081. Fax: +91-44-27480081.

10.1021/jp9046193 CCC: $40.75
Published on Web 09/09/2009

150 and 600 °C. These nanopcrystals were characterized by X-ray powder diffraction using an STOE X-ray diffractometer for phase identification and estimation of average particle size. The average sizes of the nanocrystals were obtained from the broadening of the X-ray diffraction pattern using the Scherrer formula. The transmission electron microscopy (TEM) of the nanocrystals was carried out using a Philips CM-200 microscope. The photoluminescence spectra were recorded at room temperature using a Jobin-Yvon (Fluorolog-3) spectrometer, and a xenon lamp was used as the excitation source. The Raman scattering measurements were carried out using the 532 nm line of a diode-pumped solid-state laser as the excitation and analyzed using a double-monochromator (Jobin-Yvon U1000), equipped with a liquid-nitrogen-cooled charge-coupled device (CCD) detector.

In case of perfect crystals, only the optical phonons at the zone center are involved in the first order Raman scattering process. This is because of the fact that the momentum conservation rule is valid in perfect crystals. However, in the case of nanocrystals, the lattice periodicity is interrupted at the particle surface and the phonon gets confined within the nanocrystals. Thus, the phonon wave function has to decay to a small value close to the boundary. This restriction on the phonon wave function in the real space, via a relaxation of the selection rule, allows a range of q vectors up to $\Delta q \sim \pi/d$ (d is the particle size) in the Brillouin zone to contribute to Raman scattering, resulting in a shift as well as broadening of the Raman peak. Different approaches have been used to theoretically investigate the consequences of confinement on phonon spectra. In analogy with the spatial correlation model, originally developed for disordered and amorphous materials, a Gaussian confinement model was proposed by Richter et al.[17] for spherical particles to take into account the contribution from phonons away from the zone center. This model has been further extended by Campbell and Fauchet for plate- and rod-like nanostructures.[18] This model has been extensively used to explain the Raman line shape of various nanocrystals.[19−21] According to this model, the intensity of first order Raman scattering for a nanocrystal of diameter d is

$$I(\omega, d) = \int \frac{|C(q,d)|^2}{[\omega - \omega(q)]^2 + (\Gamma_0/2)^2} d^3q \qquad (1)$$

where $\omega(q)$ is the phonon dispersion curve and Γ_0 is the natural line width of the zone-center optical phonon in bulk anatase. $C(q, d)$ is the Fourier transformation of the confinement function and is given by

$$|C(q,d)|^2 = \exp\left(\frac{-q^2d^2}{2\alpha}\right) \qquad (2)$$

A large number of results have been satisfactorily explained on the basis of the Gaussian confinement model using $\alpha = 8\pi^2$. If Δ is the width of the dispersion curve of the optical phonon, then the dispersion curve can be approximated as

$$\omega(q) = \omega_0 + \Delta \sin^2\left(\frac{qa}{2}\right) \qquad (3)$$

where ω_0 is the zone-center optical phonon frequency and a is the lattice parameter.

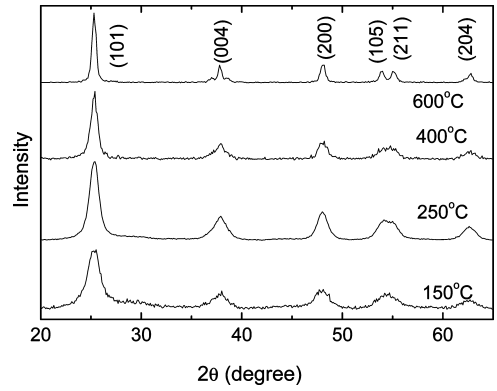

Figure 1. X-ray diffraction patterns of anatase TiO_2 nanocrystals annealed at different temperatures.

TABLE 1: Average Sizes of Anatase Nanocrystals Obtained upon Annealing As-Synthesized Powder at Different Temperatures

annealing temperature (°C)	average size (nm)
150	5.5
250	8
400	10
600	17

Results and Discussion

Nanocrystals of anatase TiO_2 of various sizes were obtained by annealing the as-synthiszed sample at different temperatures ranging from 150 to 600 °C. Figure 1 shows the powder X-ray diffraction (XRD) pattern of TiO_2 samples annealed at different temperatures. The diffraction peaks are broad and become narrower with an increase in annealing temperature. These peak positions match well with the JCPDS data for the anatase phase of TiO_2. From the XRD pattern and using the Debye−Scherrer formula, the sizes were estimated and these are given in Table 1. The average sizes of the nanoparticles were also estimated from TEM which are consistent with those estimated by XRD.

As mentioned earlier, the Raman spectrum is mainly affected by the size of nanoparticles, defects, and temperature. The temperature dependent Raman investigations have been reported both in bulk and nanocrystalline anatase TiO_2.[15,22] The effect of annealing on the microstructural evolution in nanophase TiO_2 has also been reported.[23] However, the effect of laser-induced local heating on TiO_2 nanocrystals of different sizes has not been investigated yet. In order to confirm whether the observed line broadening arises due to local heating of nanopartics, Raman spectra were investigated using several laser powers ranging from 5 to 200 mW. It is important to note that among all of the observed Raman peaks the peak at 144 cm^{-1} is most intense; hence, the effects of laser-induced local heating are analyzed by examining this peak alone. Figure 2 shows pairs of spectra recorded at the lowest and highest laser powers for different particle sizes. One can see that for 17 nm particles both the peak center and line width change only marginally at higher laser power. On the other hand, the changes in the peak position and line width are fairly larger at higher power for 5.5 nm particles. For intermediate sizes, the changes in the spectra arising at higher power lie between those of 17 and 5.5 nm. Figure 3 shows the variation of full width at half-maximum (fwhm) as a function of laser power for different nanoparticles. For larger particle size, the increase of line width is slow, whereas, for the smaller particles, the fwhm is found to increase rapidly. Larger widths at higher laser powers suggest that there could be a rise in temperature due to local heating. In order to

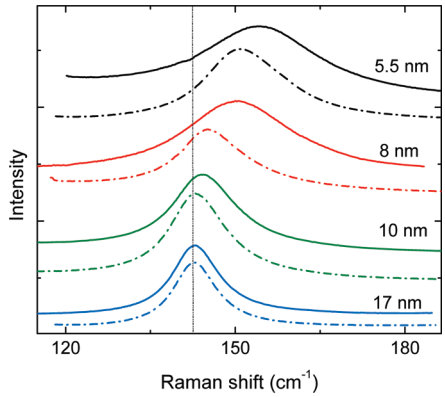

Figure 2. Raman spectra of the 144 cm^{-1} E_g phonon of TiO_2 nanocrystals at different laser powers. Dot−dash curves, 5 mW; full curves, 200 mW.

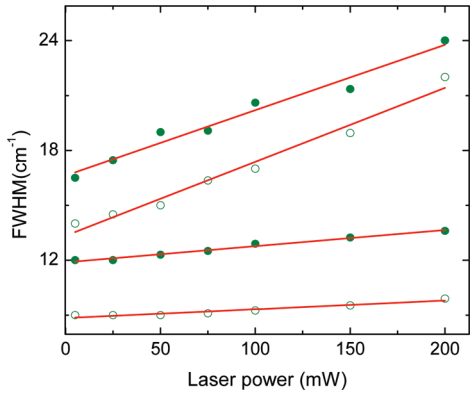

Figure 3. Full width at half-maximum of the 144 cm^{-1} E_g phonon of TiO_2 nanocrystals as a function of incident laser power. Straight lines through the data are guides to the eye.

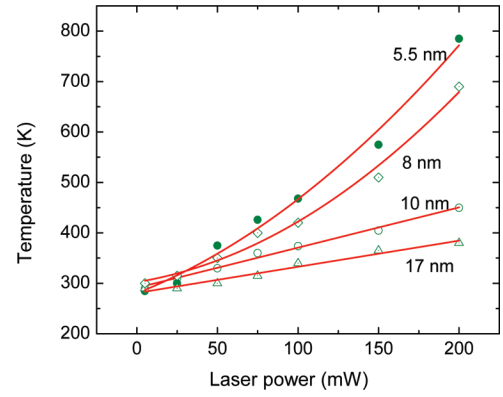

Figure 4. Calculated local Raman temperature of TiO_2 nanocrystals versus incident laser power. Solid curves through the data are guides to the eye.

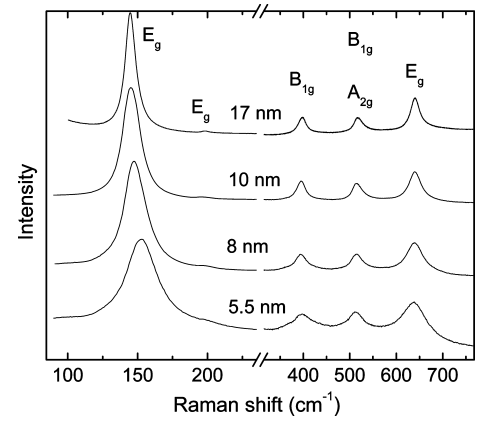

Figure 5. Complete Raman spectra of TiO_2 nanocrystals recorded at 5 mW incident laser power.

confirm this, the local temperature of the nanoparticles at different laser powers was estimated from the Stokes to anti-Stokes intensity ratio of the first order Raman spectra. The intensity ratio is given as[24]

$$\frac{I_s}{I_{as}} = K \exp\left(\frac{\hbar\omega}{K_B T}\right) \quad (4)$$

where I_s and I_{as} are the Stoke and anti-Stoke intensity. The constant K is often different from 1 if the absorption coefficients for the Stokes and anti-Stokes wavelengths are different.[25] The value of K is estimated from the Stokes and anti-Stokes intensity ratio for 5 mW laser power by assuming the local temperature of nanoparticles to be room temperature at this laser power. This is reasonable because further reduction in laser power below 5 mW did not result in any change in peak position and fwhm for all samples. Figure 4 shows the variation of estimated Raman temperature with incident laser power for nanoparticles of different sizes. As expected, the Raman temperature increases with an increase in laser power. From Figure 4, we also find that for any given power local heating is more for the smaller particles than the bigger particles. This confirms that laser-induced increased broadening of the Raman spectra of smaller particles indeed arises due to local heating at higher laser power. Similar behavior has also been observed in germanium nanowires by Jalilian et al.[26] For a given laser power, the nanowires with smaller diameter showed larger broadening and larger down-shifted Raman spectra as compared to large diameter nanowires. The estimated local temperature was also highest for wires of lowest diameter. It is important to note that the power dependent laser heating is strongly related to the laser spot size. For example, in experiments performed using a micro-Raman setup (laser spot ~1 μm), even a power of a few milliwatts can cause a high local temperature of the sample.[24,25] Therefore, it is important to eliminate the thermal effect on the Raman line shape arising from laser-induced local heating before analyzing the effect of phonon confinement in anatase nanocrystals. Hence, only the spectra recorded with 5 mW power were used for the quantitative analysis based on the phonon confinement model.

Figure 5 shows the Raman spectra of TiO_2 nanoparticles of different sizes. Five peaks are observed at around 144, 200, 397, 516, and 639 cm^{-1} in all samples, and these peaks are assigned as E_g, E_g, B_{1g}, (B_{1g}/A_{1g}), and E_g modes, respectively. Due to the very weak intensity of the 200 cm^{-1} E_g phonon, it is not possible to analyze its line shape. On the other hand, the mode frequencies of both B_{1g} and A_{1g} modes are very close to 516 cm^{-1}. As a result, it is difficult to separate the contributions of each of these modes to the 516 cm^{-1} peak. Hence, only the unambiguous modes at 144, 397, and 639 cm^{-1} are considered for a detailed line shape analysis in anatase nanoparticles. One can see from Figure 5 that a distinct blue shift of peak position of the 144 cm^{-1} E_g phonon mode occurs for nanoparticles of smaller sizes. The 639 cm^{-1} E_g and 397 cm^{-1} B_{1g} modes also shift with a decrease in particle size. However, their shifts are significantly smaller than that of the 144 cm^{-1} mode. One can also see that the Raman spectra show a systematic asymmetric broadening with decreases in the nanoparticle size. These

TABLE 2: Intrinsic Full Widths at Half-Maximum (Γ_0) and Widths of the Bulk Dispersion Curves (Δ) of Anatase TiO_2 Used in the Calculation of the Raman Line Shape of Different Modes[a]

				Γ_b (cm^{-1})		
mode	ω_0 (cm^{-1})	Γ_0 (cm^{-1})	Δ (cm^{-1})	5.5 nm	8 nm	10 nm
E_g	144	7.5	+200	13.5	10	9
B_{1g}	397	20	−150	35	25	20
E_g	639	20	+190	43	30	23

[a] Γ_b is the fwhm that gives good agreement between the spectra and the calculated line shape.

changes arise due to phonon confinement.[27] We now analyze the line shapes of all three phonons using a phonon confinement model.

There are several reports on phonon confinement in anatase TiO_2 nanocrystals, and most of them have used the value of Δ either arbitrarily or have used that of the rutile phase.[6,7] There is no experimental data available for the phonon dispersion relation for anatase TiO_2. However, Mikami et al. have recently reported a theoretical calculation of phonon dispersion for anatase TiO_2.[28] Bassi et al. have used the Δ obtained from this calculation.[5] They also examined the effect of the anisotropic dispersion curve of the 144 cm^{-1} E_g mode on the phonon line width. Although the calculated linewidths agreed with the data, the nanocrystalline samples contain both anatase and rutile phases. As mentioned earlier, the 144 cm^{-1} E_g mode has the same frequency as that of the B_{1g} mode of rutile. Consequently, in a two-phase sample, the 144 cm^{-1} Raman peak can have a contribution from both of these modes. Hence, analysis of line width data of a two-phase system based on the phonon dispersion curve of a single phase appears inappropriate. A recent study by Balaji et al. has also examined the phonon confinement effect in nanocrystalline anatase.[4] They consider the anisotropy of two branches of the 144 cm^{-1} E_g mode along the $\Gamma-N$ direction and have given equal weightage to these branches in the calculation, whereas the branch along the $\Gamma-X$ direction with the largest dispersion curve was ignored. In anisotropic phonon dispersion, the branch with the largest dispersion should contribute the maximum to the Raman line shape and hence cannot be ignored. In the present calculation, we used the value of Δ for the most dispersive branch along the $\Gamma-X$ direction found in the calculated phonon dispersion curve.[28] Table 2 lists the values of Γ_0 and Δ of different optical phonons, used for the calculation of phonon line shapes for nanoparticles of different sizes, which are taken from the earlier reported results on TiO_2.[22,28]

It may be pointed out that eq 1 represents the line shape for a given size. On the other hand, a wide distribution of particle size can significantly modify the Raman line shape. The actual particle size distribution can be taken into account by summing over the contributions from all sizes in the following manner. The contribution of size distribution to the Raman line broadening can be obtained by

$$I(\omega) = \sum_i P(d_i) I(\omega_i d_i) \qquad (5)$$

where $P(d_i)$ is the normalized discrete size distribution ($\sum_i P(d_i) = 1$). Figure 6 compares the calculated total Raman line broadening for the 250 °C annealed sample by taking the average size estimated from XRD and the size distribution obtained from TEM. The bright-field TEM image and the size distribution are shown as insets in Figure 6. The average particle size is 8.8 nm with a standard deviation of 0.75 nm which is consistent with the XRD result. One can see that both of the calculated spectra differ only marginally from each other due to the narrow size distribution. Other samples show a similar result. Hence, in view of the close agreement between the line shape obtained by taking the average size from XRD and the size distribution from TEM, all calculations are carried out by considering the sizes obtained by XRD.

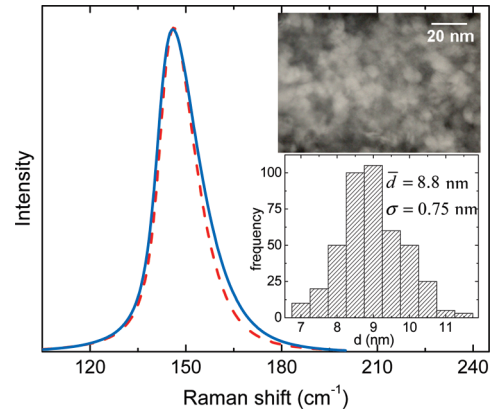

Figure 6. Comparison between the calculated Raman line shapes obtained by taking the average particle size from XRD (full curve) and the actual particle size distribution obtained from TEM (dashed curve) for the 250 °C annealed sample. The insets show the histogram of the particle size distribution and a bright-field TEM image.

Figure 7 compares the calculated confined phonon line shapes with the measured Raman spectra for different particle sizes. One can see that the data and calculated profiles do not match well for all three phonons for smaller particle sizes, with the disagreement being least for the 144 cm^{-1} E_g mode and largest for the 397 cm^{-1} B_{1g} mode. The experimental line shapes for all of the phonon modes are broader than the calculated profiles. In order to obtain reasonable agreement between the calculated and measured spectra of the 144 cm^{-1} E_g mode, the Raman line shapes for nanocrystals of different sizes were recalculated using increased natural line widths Γ_b and the calculated profiles are also shown as full curves in Figure 7. Similar analyses were also carried out for the 397 cm^{-1} B_{1g} and 639 cm^{-1} E_g modes, and the results are included in Figure 6. One can see that good fits to the data are possible using larger intrinsic widths Γ_b. The values of Γ_b that yield good agreement are also given in Table 2. The full width at half-maximum of the measured Raman spectra and those calculated using the phonon confinement model for different modes are compared in Figure 8 as a function of particle size. One can see that for larger size particles there is a good agreement between the measured linewidths and those predicted by the phonon confinement model. On the other hand, for small particles, there is a significant difference between the two and one has to necessarily use larger intrinsic widths to get a good fit to the measured spectra.

We now discuss the possible reasons for larger line widths of the spectra than those predicted by the phonon confinement model for smaller particle sizes for different phonon modes. We first examine if surface phonons can give rise to additional intensity in the wings. The surface phonons in polar crystal are found between transverse optical (TO) and longitudinal optical (LO) mode frequencies.[29] However, in the case of TiO_2, the Raman active E_g and B_{1g} modes are nonpolar and hence do not have an associated macroscopic electric field. Only the infrared active polar modes exhibit LO−TO splitting and are expected to have surface phonons.[30] The other possible reason for the

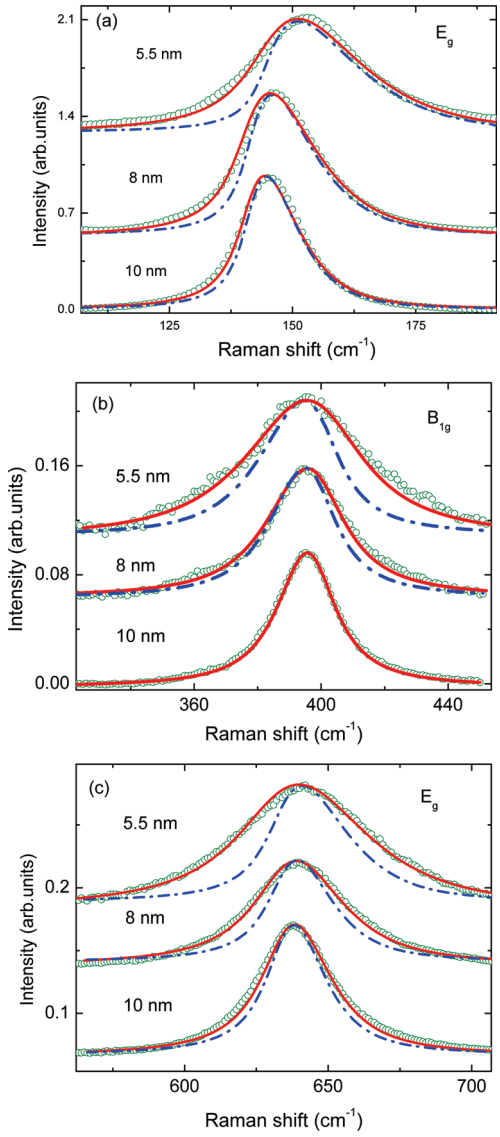

Figure 7. Comparison of Raman spectra of different phonons with the line shape predicted by the phonon confinement model. Open symbols, data; dot−dash curve, calculated line shape using Γ_0 as the fwhm; solid curves, calculated line shape using Γ_b as the fwhm. (a) 144 cm^{-1} E_g mode, (b) 397 cm^{-1} B_{1g} mode, and (c) 639 cm^{-1} E_g mode.

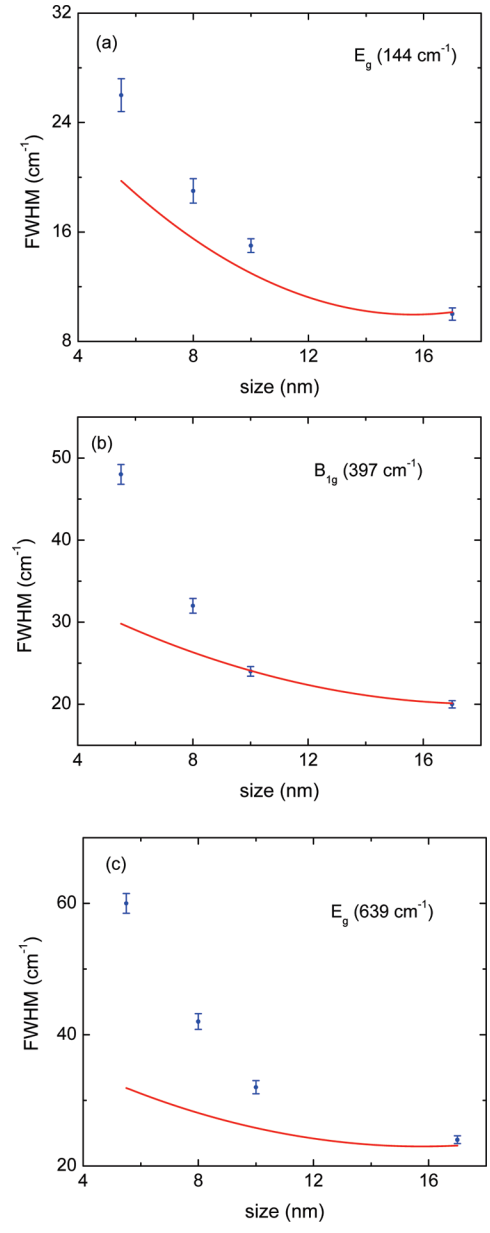

Figure 8. Comparison of the fwhm of the Raman spectra of E_g and B_{1g} phonons of TiO_2 nanocrystals with that obtained from the phonon confinement model using Γ_0 as intrinsic widths. Filled symbols are the measured fwhm of the spectra, and solid curves represent the widths of the calculated profiles. (a) 144 cm^{-1} E_g mode, (b) 397 cm^{-1} B_{1g} mode, and (c) 639 cm^{-1} E_g mode.

extra broadening of the Raman line shape could be due to the presence of defects in small nanocrystals. As-synthesized samples upon annealing at relatively lower temperature such as 150 °C result in the formation of small nanocrystals. These nanocrystals are not expected to be free from defects. The defects scatter phonons, causing their decay and consequent decrease in their lifetime. This results in an increase in phonon line width. Thus, the defects cause symmetric broadening of Raman spectra.[31] This implies that 5.5 nm diameter anatase nanocrystals obtained upen annealing at 150 °C have a substantially large concentration of defects. The present result suggests that, as the sample is annealed at successively higher temperatures, in addition to an increase of the average particle size, the defect concentration also reduces substantially. Annealing at 600 °C finally results in nearly defect free nanocrystals. If one examines the difference between Γ_0 and Γ_b for 5.5 nm anatase nanocrystals, it is found that, among the phonons studied in the present work, the 397 cm^{-1} B_{1g} and 639 cm^{-1} E_g modes show a much larger disagreement as compared with the 144 cm^{-1} E_g mode. This suggests that these modes are more sensitive to the presence of defects as compared to the most intense 144 cm^{-1} E_g mode studied by other researchers earlier.[4−7]

A discussion on the nature of defects is in order. Often, the observed broadening and shift of the 144 cm^{-1} E_g mode is tentatively attributed to oxygen related "stoichiometry defects".[5] This is because a departure of oxygen stoichiometry from 2.00 has been reported to cause broadening and a blue shift of as much as 10 cm^{-1} of the strongest E_g mode at a stoichiometry of 1.89.[32] In addition, accompanying dramatic changes in the optical properties, in terms of the colors of the sample, were also found;[32] i.e., the color changes from white to pale yellow to light blue to dark blue as the oxygen stoichiometry varied from 2 to 1.89. On the other hand, all of the present samples were white in color, suggesting that the present sol−gel method resulted in stoichiometric TiO_2 and oxygen deficiency related

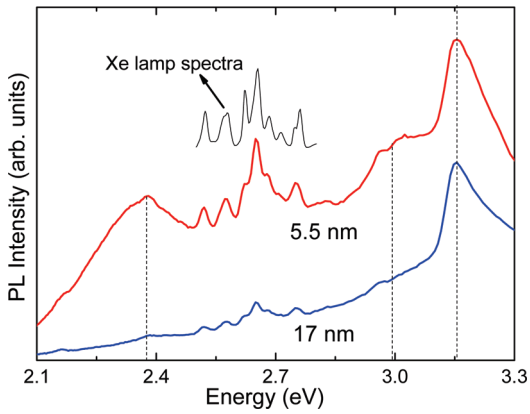

Figure 9. Comparison of room temperature photoluminescence spectra of 5.5 and 17 nm TiO_2 nanocrystals. The dashed vertical lines corrospond to the energies of PL emission from TiO_2 nanocrystals. The peaks between 2.5 and 2.8 eV arise due to the xenon lamp.

defects were not the cause of extra broadening of Raman spectra in small nanocrystals. This suggests that the defects responsible for broadening of the Raman line shape are intrinsic defects. On the other hand, TiO_2 nanocrystals formed using other synthesis methods such as flame pyrolysis[5] and the inert gas condensation method[32] led to oxygen deficient nanocrystals.

In order to examine if annealing changes the defect concentration, room temperature photoluminescence (PL) spectra of samples annealed at different temperatures were recorded. Figure 9 compares the PL spectra of the smallest (5.5 nm) and largest (17 nm) size nanocrystals. A distinct peak at around 3.15 eV is observed in all samples. In addition, two broad peaks are also observed for smaller size at around 2.3 and 2.98 eV. A set of sharp peaks found between 2.5 and 2.8 eV arise due to the xenon lamp spectrum, also shown in Figure 9. The peak at 3.15 eV cannot be attributed to band-to-band transition, as one expects a higher value of band-to-band transition energy for nanocrystals. Hence, this transition can be assigned to free exciton recombination below the conduction band.[33] The intensity of the peak at 2.98 eV decreases with an increase in particle size. This peak has been assigned as self-trapped exitons localized at TiO_6 octahedra in TiO_2 (each Ti^{4+} is surrounded by six O^{2-} ions).[34] The peak at 2.3 eV has the largest intensity for the smallest particle size, and with an increase in annealing temperature, the intensity decreases systematically. This broad peak is usually observed in smaller nanocrystals and has been assigned as surface states formed by Ti^{3+} on the surface of small nanocrystals.[35] In nanocrystals, due to the large surface to volume ratio, it is expected that surface states are formed by ion vacancy or surface ions with less coordination number. These surface states acts as the luminescence center. With an increase in annealing temperature (increase in particle size), these defects are annealed out. A significant decrease in defect PL intensity with an increase in nanoparticle size in anatase TiO_2 has been reported,[36] consistent with the present findings.

Conclusions

Anatase nanocrystals of different sizes have been synthesized by the sol−gel technique followed by annealing at different temperatures. Raman spectra of phonons of E_g (144 and 639 cm^{-1}) and B_{1g} (397 cm^{-1}) symmetries are quantitatively analyzed in 5.5, 8, 10, and 17 nm nanocrystals using a phonon confinement model. A laser-induced local heating is found to cause significant line broadening and peak shift in TiO_2 nanocrystals of different sizes. It is also found that smaller particles exhibit higher local temperature than the larger ones. The experimental Raman line shapes are found to be broader than those predicted by a confinement model for smaller nanocrystals. The extra broadening of the experimental line shape is attributed to the presence of defects in TiO_2 nanocrystals. Upon annealing, the defect concentration decreases and its contribution to Raman line broadening become less significant. Consequently, for higher particle size, the calculated Raman profile agrees with the measured spectra. Furthermore, the contribution of defects to the broadening for the 397 cm^{-1} B_{1g} and 639 cm^{-1} E_g modes is found to be much more than that for the 144 cm^{-1} E_g mode. Thus, the present results show that the phonon confinement effects are different for phonons of different symmetries in anatase nanocrystals, and while analyzing the Raman spectra of small nanocrystals, one needs to take into account the local temperature and defects in addition to those arising from phonon confinement and departure from stoichiometry.

Acknowledgment. The authors gratefully acknowledge Dr. Saroja Saibaba and Dr. Arup Dasgupta for obtaining the TEM micrographs and Mrs. Annalakshmi for obtaining the PL spectra. The authors thank Dr. C. S. Sundar for interest in the work and Dr. Baldev Raj for support and encouragement.

References and Notes

(1) O'Regan, B.; Gratzel, M. *Nature (London)* **1991**, *353*, 737.
(2) Bach, U.; Lupo, D.; Comte, P.; Moser, J. E.; Weissortel, F.; Salbeck, J.; Spreitzer, H.; Gratzel, M. *Nature (London)* **1998**, *395*, 583.
(3) Lottici, P. P.; Bersani, D.; Braghini, M.; Montenero, A. *J. Mater. Sci.* **1993**, *28*, 177.
(4) Balaji, S.; Djaoued, Y.; Robichaud, J. *J. Raman Spectrosc.* **2006**, *37*, 1416.
(5) Li Bassi, A.; Cattaneo, D.; Russo, V.; Bottani, C. E.; Barborini, E.; Mazza, T.; Piseri, P.; Milani, P.; Ernst, F. O.; Wegner, K.; Pratsinis, S. E. *J. Appl. Phys.* **2005**, *98*, 074305.
(6) Bersani, D.; Lottici, P. P.; Ding, X. Z. *Appl. Phys. Lett.* **1998**, *72*, 73.
(7) Ivanda, M.; Music, S.; Gotic, M.; Turkovic, A.; Tonejc, A. M.; Gamulin, O. *J. Mol. Struct.* **1999**, *480−481*, 641.
(8) Melendres, C. A.; Narayanasamy, A.; Maroni, V. A.; Siegal, R. W. *J. Mater. Res.* **1989**, *4*, 1246.
(9) Rajalakshmi, M.; Arora, A. K.; Bendre, B. S.; Mahamuni, S. *J. Appl. Phys.* **2000**, *87*, 2445.
(10) Spanier, J. E.; Robinson, R. D.; Zhang, F.; Chan, S. W.; Herman, I. P. *Phys. Rev. B* **2001**, *64*, 245407.
(11) Balkanski, M.; Wallis, R. F.; Haro, E. *Phys. Rev. B* **1983**, *28*, 1928.
(12) Alim, K. A.; Fonoberov, V. A.; Balandin, A. A. *Appl. Phys. Lett.* **2005**, *86*, 053103.
(13) Klemens, P. G. *Phys. Rev.* **1966**, *148*, 845.
(14) Ridley, B. K. *J. Phys.: Condens. Matter* **1996**, *8*, L511.
(15) Du, Y. L.; Deng, Y.; Zhang, M. S. *J. Phys. Chem. Solids* **2006**, *67*, 2405.
(16) Li, G.; Li, L.; Boerio-Goates, J.; Woodfield, B. F. *J. Am. Chem. Soc.* **2005**, *127*, 8659.
(17) Richter, H.; Wang, Z. P.; Ley, L. *Solid State Commun.* **1981**, *39*, 625.
(18) Campbell, I. H.; Fauchet, P. M. *Solid State Commun.* **1986**, *58*, 739.
(19) Sahoo, S.; Dhara, S.; Mahadevan, S.; Arora, A. K. *J. Nanosci. Nanotechnol.* **2009**, *9*, 5604.
(20) Paillard, V.; Puech, P.; Laguna, M. A.; Carles, R.; Kohn, B.; Huisken, F. *J. Appl. Phys.* **1999**, *86*, 1921.
(21) Nandakumar, P.; Vijayan, C.; Rajalakshmi, M.; Arora, A. K.; Murti, Y. V. G. S. *Physica E* **2001**, *11*, 377.
(22) Ohsaka, T. *J. Phys. Soc. Jpn.* **1980**, *48*, 1661.
(23) Eastman, J. A. *J. Appl. Phys.* **1994**, *75*, 770.
(24) Gupta, R.; Xiong, Q.; Adu, C. K.; Kim, U. J.; Eklund, P. C. *Nano Lett.* **2003**, *3*, 627.
(25) Niu, J.; Sha, J.; Yang, D. *Scr. Mater.* **2006**, *55*, 183.
(26) Jalilian, R.; Sumanasekera, G. U.; Chandrasekharan, H.; Sunkara, M. K. *Phys. Rev. B* **2006**, *74*, 155421.
(27) Arora, A. K.; Rajalakshmi, M.; Ravindran, T. R.; Sivasubramanianm, V. *J. Raman Spectrosc.* **2007**, *38*, 604.
(28) Mikami, M.; Nakamura, S.; Kitao, O.; Arakawa, H. *Phys. Rev. B* **2002**, *66*, 155213.

(29) Sahoo, S.; Hu, M. S.; Hsu, C. W.; Wu, C. T.; Chen, K. H.; Chen, L. C.; Arora, A. K.; Dhara, S. *Appl. Phys. Lett.* **2008**, *93*, 233116.
(30) Warren, D. S.; McQuillan, A. J. *J. Phys. Chem. B* **2004**, *108*, 19373.
(31) Sahoo, S.; Dhara, S.; Sivasubramanian, V.; Kalavathi, S.; Arora, A. K. *J. Raman Spectrosc.* **2009**, *40*, 1050.
(32) Parker, J. C.; Siegel, R. W. *Appl. Phys. Lett.* **1990**, *57*, 943.
(33) Zhang, Y.; Wu, L.; Xie, E.; Duan, H.; Han, W.; Zhao, J. *J. Power Sources* **2009**, *189*, 1256.
(34) Lei, Y.; Zhang, L. D.; Meng, G. W.; Li, G. H.; Zhang, X. Y.; Liang, C. H.; Chen, W.; Wang, S. X. *Appl. Phys. Lett.* **2001**, *78*, 1125.
(35) Yu, J. C.; Yu, J. G.; Ho, W. K.; Jiang, Z. T.; Zhang, L. Z. *Chem. Mater.* **2002**, *14*, 3808.
(36) Zhao, Y.; Li, C.; Liu, X.; Gu, F.; Jiang, H.; Shao, W.; Zhang, L.; He, Y. *Mater. Lett.* **2007**, *61*, 79.

JP9046193